

The work reported in this document was performed at Lincoln Laboratory, a center for research operated by Massachusetts Institute of Technology, with the support of the U.S. Air Force under Contract AF 19(628)-500.

Non-Lincoln Recipients

PLEASE DO NOT RETURN

Permission is given to destroy this document
when it is no longer needed.

DDC release to OTS is not authorized.

MASSACHUSETTS INSTITUTE OF TECHNOLOGY

LINCOLN LABORATORY

PROJECT WEST FORD PAYLOAD TELEMETRY SYSTEM

W. T. HIGGINS

L. A. JACOBSON

Group 63

J. B. RANKIN

Group 61

TECHNICAL REPORT 343

20 JANUARY 1964

LEXINGTON

MASSACHUSETTS

ABSTRACT

The beacon track and performance telemetry system used in the various Project West Ford communication payloads is described. The dispense dispensing rate, the dispenser spin, tumble and temperature, as well as the system power-supply voltage, were measured and transmitted to the West Ford sites by means of a pulse-duration modulation system. In addition, the telemetry transmitter served as a beacon for accurate ground-based radar tracking of the payloads. The most important system considerations were efficiency, low power, simplicity, and high reliability. A tabulation of the received data and the interpretation of the data are given.

Accepted for the Air Force
Franklin C. Hudson, Deputy Chief
Air Force Lincoln Laboratory Office

TABLE OF CONTENTS

Abstract	iii
I. INTRODUCTION	1
II. GENERAL CONSIDERATIONS	3
A. System Approach	3
B. Sensors	6
III. LOGIC CIRCUITRY	9
A. Functional Design	9
B. Circuits	10
IV. TELEMETRY TRANSMITTER	15
V. TELEMETRY ANTENNA AND MATCHING NETWORK	18
A. Electrical Design	20
B. Experimental Adjustment of Variables	23
C. Performance	25
VI. MECHANICAL	27
VII. RESULTS	28
APPENDIX A – Round Canister	31
APPENDIX B – Modified Square Canister	32
APPENDIX C – Logic Circuitry Considerations	34
I. One-Shot Multivibrator Power	34
II. Dispensing Rate Timing Circuit	34
APPENDIX D – Antenna Phasing Network	37

PROJECT WEST FORD PAYLOAD TELEMETRY SYSTEM

I. INTRODUCTION

A payload telemetry canister was added to the Project West Ford experiment to facilitate tracking and to provide for the acquisition of performance data concerning the dipole dispenser. The canister was mounted directly against two dipole disks so that they and the other four dipole packages could be located quickly and accurately once they had been ejected. The dipole-dispensing rates, the rotational velocities, and the disk temperatures were measured and telemetered to the ground receiving stations.

The canister was designed to transmit at a minimum peak power of 100 mw at 240 Mcps. The following five measurements were encoded in the telemetered beacon:

- Spin rate
- Dispensing rate of the dipoles
- Temperature
- Tumble rate
- Canister supply voltage.

The ejection mechanism operated so that all dipole packages (including the two disks with the canister) would, initially, have the same angular velocity about their axes of circular symmetry. The knowledge of this spin rate is important because it influences the quality and the rate of dipole dispensing.

The sublimation rate of the naphthalene bonding the dipoles together and the dipole dispensing rate have a strong temperature dependence. Knowledge of temperature is important in comparing actual dispenser performance with designed performance. The tumble measurement provides an indication of any rotation about an axis other than the intended axis (axis of circular symmetry).

Monitoring the canister supply voltage provides a check on the accuracy of the other telemetered information and provides a record of the rate of battery discharge.

Constraints:- The following constraints were necessitated by the integration of the canister with the experiment and by the expected environmental conditions encountered in orbit:

- Allowed volume approximately 100 in.³ ($4\frac{1}{2} \times 4\frac{1}{2} \times 5$)
- Self-contained power supply
- Temperature range of operation, -50° to $+50^{\circ}\text{C}$
- Self-contained sensors

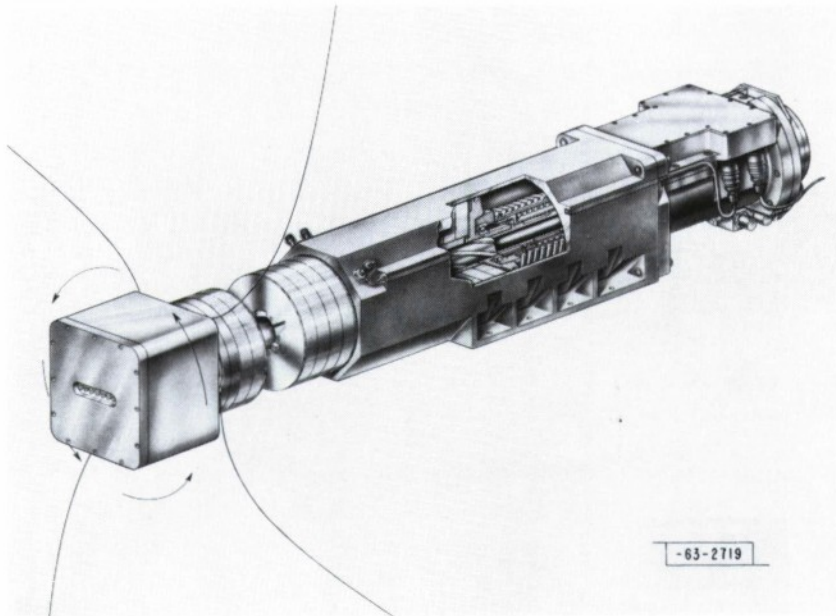


Fig. 1. X-band dipole dispenser - Mk II.

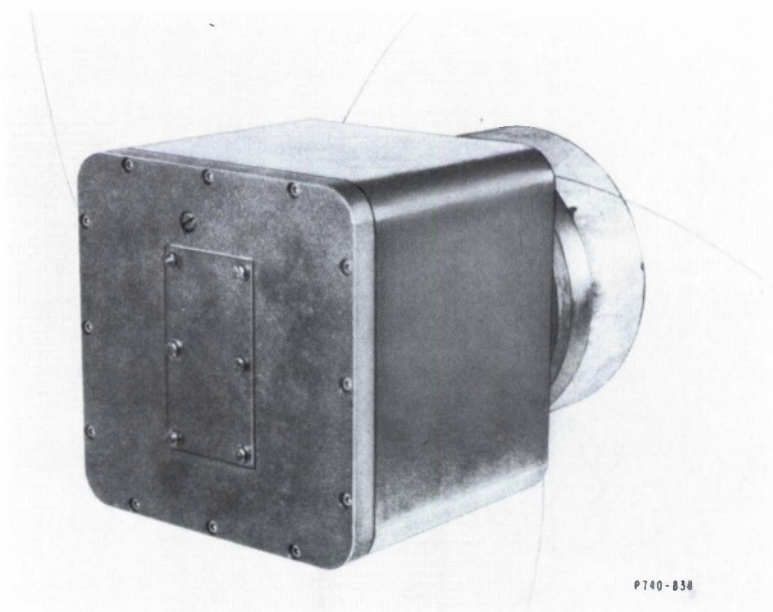


Fig. 2. West Ford telemetry canister.

Near omnidirectional antenna pattern
 Minimum life of operation, 170 hours
 Ability to meet vehicle test specifications (especially vibration and acceleration).

There were no weight requirements other than those imposed by the volume restriction.

This report describes in detail the canister, now referred to as the "square" canister, which was designed to meet the preceding requirements and constraints. Two other models of the canister, which had slightly different objectives and which were subjected to slightly different constraints, are discussed briefly in Appendices A and B.

The X-band dipole dispenser and the West Ford telemetry canister are shown in Figs. 1 and 2, respectively.

II. GENERAL CONSIDERATIONS

A. System Approach

Volume and system-life considerations ruled out CW telemetry. The following example will show why. A 15-percent-efficient solid-state transmitter operated at the minimum output power of 100 mw would require over 100 watt-hours of energy to run for 170 hours; whereas a 100-in.³ pack of the most efficient batteries available (silver-zinc cells) would supply but 75 watt-hours. Thus, if the entire allowable volume were occupied by batteries, CW operation would not be possible for the required time. Therefore a duty-cycle approach was necessitated.

To obtain the duty cycle used, the following formula was applied:

$$\frac{V_b \times E_d \times \% B_t \times E_{ff}}{P_p \times T_m \times S_f} = \% \text{ duty cycle} \quad . \quad (1)$$

The following values were taken for these quantities:

	<u>Symbol</u>	<u>Value</u>
Effective volume of batteries	V_b	50 in. ³
Energy density of silver-zinc batteries	E_d	0.75 watt-hour/in. ³
Percent of batteries used for transmitter	$\% B_t$	80%
Efficiency of transmitter	E_{ff}	0.15
Highest peak power	P_p	0.250 watt
Minimum operating life	T_m	170 hours
Safety factor	S_f	4

The safety factor of 4 was chosen to allow battery degradation, due to possible prolonged launch holds, and to permit operation at very low temperatures. Substitution of these values in Eq. (1) gives a duty cycle of:

$$\frac{50 \times 0.75 \times 80 \times 0.15}{4 \times 0.250 \times 170} = 2.6 \text{ percent} \quad . \quad (2)$$

It was decided that pulse-duration modulation would be employed because it is a simple type of modulation to implement and to receive. This encoding system minimizes on-board circuitry, which in turn helps retain high reliability.

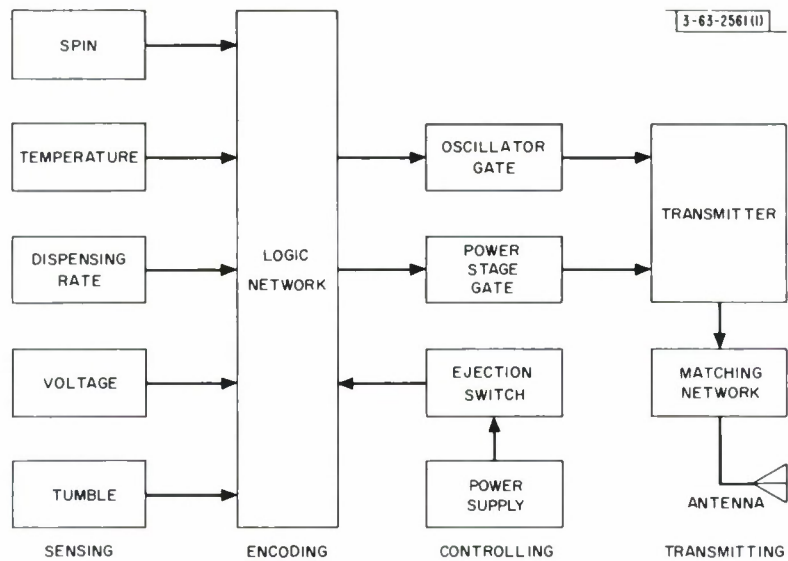


Fig. 3. System block diagram.

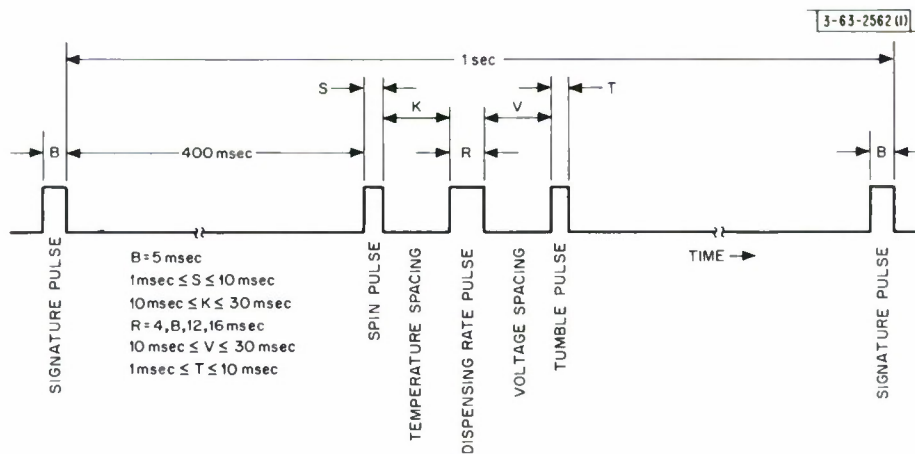


Fig. 4. Telemetry output format.

Two main criteria influenced the selection of the pulse encoding once the duty cycle was specified. The first was that pulse widths should be long enough so that the received signal would approximate a line spectrum. This would permit the use of narrow-band filters in the receiver. The second, but contrasting constraint, was that the pulse repetition rate should be as high as possible to facilitate tracking. Thus, it was decided to make the pulses as short as possible while still satisfying the first criterion.

The receiving system was to contain a "comb filter" consisting of, among other things, a bank of 10-kcps filters. In this system the output of the 10-kcps filter which contains the strongest signal is retained, and the outputs of the other 10-kcps filters are suppressed.

If the carrier frequency were in the center of the frequency band of one of the 10-kcps filters, the receiver output rise time would be approximately:

$$\frac{2}{3} \times \frac{1}{f_1} = \frac{2}{3} \frac{1}{10^4} = 65\text{-}\mu\text{sec rise time} \quad (3)$$

When the frequency is not centered in the filter the rise time will be longer.

It is not the rise time itself that contributes pulse-width measurement error but, rather, the uncertainty in it. Assuming that the probability distribution function of the received frequency is flat with respect to its position in the 10-kcps filter and that the 10-kcps filters are not ideal, the rise time has an uncertainty comparable to the center frequency rise time. This results in an error in the reading of the pulse widths on the order of 50 μ sec. The fall time, being solely dependent upon the filter characteristics, has negligible error associated with it. This implies that for a minimum accuracy of about 5 percent all pulse widths should be greater than 1 msec.

This pulse width was also compatible with the quick-look data recorder, since this recorder had a resolution of about $\pm 100 \mu$ sec. With the presence of a signal which is large compared to the system noise the filter output has a 50- μ sec accuracy; whereas the quick-look data have an over-all resolution somewhat greater than 100 μ sec.

If the information pulses have a range of from 1 to 10 msec with a resolution of 50 μ sec, a dynamic range of about 200 is achieved. $N/2$ pulses are necessary to carry N channels of transmitted information using pulse duration modulation (PDM) techniques since both the pulse widths and pulse spacings can carry information. Another way of envisioning this information content is by noting that both the leading and falling edges of the pulses provide information. In this system there are six channels of information: spin rate, dispensing rate, temperature, tumble rate, on-board voltage, and a time-reference identification point. Thus three pulses were necessary for the telemetry encoding. The most important information channels, namely, spin rate, dispensing rate, and tumble rate were encoded in a positive fashion with the pulse widths. Temperature, voltage, and time reference were encoded as pulse spacings.

An expected total pulse width less than 15 msec was achieved by choosing each pulse width so that it was as small as possible for the expected indication of its sensor. A fourth 5-msec pulse, which contained no sensor information, was added for reasons discussed in Sec. III-A. This brought the expected total pulse width to less than 20 msec with a total maximum of about 35 msec. An over-all cycle time of one second gave an expected duty cycle of less than 2 percent as compared to the desired 2.6 percent. The unlikely (3.5-percent) duty cycle is still well within the design range as protected by the safety factor of 4.

The system block diagram of the telemetry canister is shown in Fig. 3 and the telemetry output format is shown in Fig. 4.

The placing of the three pulses in close proximity with respect to each other aided in the instrumentation of the encoding and facilitated data reduction. The pulse spacings were made wider than the pulses to increase the resolution in these spacings.

B. Sensors

Rotational parameters of the canister are inferred through the use of accelerometers. Gyroscopes, or other direct rotation-sensing elements, dissipate prohibitive amounts of power and do not lend themselves to pulse-width encoding as readily as the varying resistance of an accelerometer.

Figure 5 shows the placement of two orthogonally mounted accelerometers designated "spin accelerometer" (indication is maximum when the rotation axis and z-axis are coincident) and "tumble accelerometer" (indication is minimum when rotation axis and z-axis are coincident).

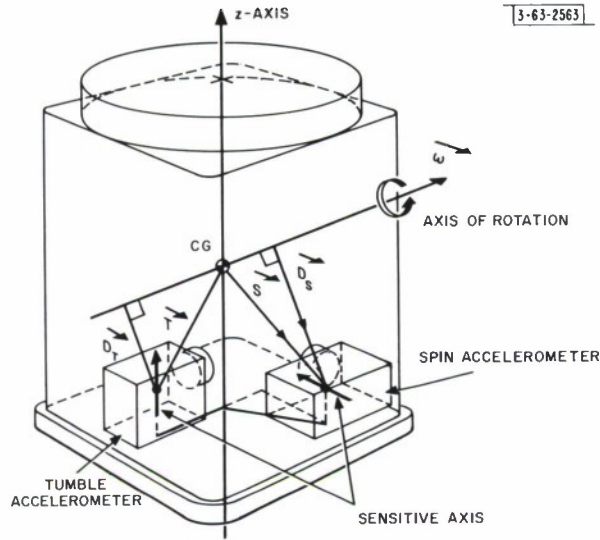


Fig. 5. Placement of accelerometers.

The acceleration A_s , as indicated by the spin accelerometer, is the cross product of the radial acceleration at the spin accelerometer and the unit direction vector \vec{i}_x where:

$\vec{\omega}$ = rotation vector of canister,

\vec{S} = spin accelerometer position vector with respect to c.g. position,

\vec{T} = tumble accelerometer position vector with respect to c.g.

This radial acceleration is $\omega^2 D_s$, where \vec{D}_s is the shortest vector between the rotational axis and the spin accelerometer, i.e.,

$$\vec{D}_s = \vec{S} - \frac{(\vec{S} \cdot \vec{\omega})}{|\vec{\omega}|^2} \vec{\omega} \quad (4)$$

Therefore,

$$A_s = \vec{i}_x \cdot [\vec{S} \omega^2 - (\vec{S} \cdot \vec{\omega}) \vec{\omega}] \quad (5)$$

Note that A_s can be equal to zero even though ω is not zero if either $(\vec{S} \cdot \vec{\omega}) \vec{\omega} = \omega^2 \vec{S}$ or $\vec{i}_x \cdot \vec{\omega} = |\vec{\omega}|$. In other words, A_s is zero if the rotational axis passes through the accelerometer

or if it is parallel to the sensitive axis of the accelerometer. If the rotational axis lies between these two zero points, A_s assumes a negative value. The accelerometers have but one polarity and will give a zero indication for negative acceleration. Therefore the negative acceleration region is detected as a null acceleration region. Similarly, the tumble acceleration indication is

$$A_t = \vec{i}_z \cdot [\vec{T} \omega^2 - (\vec{T} \cdot \vec{\omega}) \vec{\omega}] \quad (6)$$

This acceleration also has a null region between $\vec{T} \omega^2 = (\vec{T} \cdot \vec{\omega}) \vec{\omega}$ and $\vec{\omega} \cdot \vec{i}_z = |\omega|$.

If it is assumed that most of the rotational energy is in the form of spin then $\vec{\omega}$ can be approximated by $\vec{\omega} \approx |\vec{\omega}| \vec{i}_z + \Delta\omega \vec{i}_T$, where $\Delta\omega \vec{i}_T$ indicates the non \vec{i}_z component of $\vec{\omega}$. Then, Eq. (5) becomes

$$A_s \approx \vec{i}_x \cdot S \omega^2 + \Delta\omega \omega \vec{i}_x \cdot \vec{i}_t (S \cdot \vec{i}_z) \quad (7)$$

or

$$A_s \approx S_x \omega^2 \quad \text{for } \Delta\omega \ll \omega \text{ with an error } \leq |\Delta\omega \omega S_z| \quad (8)$$

where $S_x = \vec{i}_x \cdot S$ or is equal to the x displacement between the spin accelerometer and the c.g., and $S_z = \vec{i}_z \cdot S_x$. ω can now be recovered quite accurately from Eq. (8) alone.

Under this assumption Eq. (6) becomes

$$\begin{aligned} A_t &\approx -\Delta\omega \vec{i}_t \cdot (\vec{T} - \vec{T}_z) \omega \leq \Delta\omega \omega T_t \\ A_t &\approx T_z \omega^2 - T_z \omega^2 - \omega \Delta\omega T = \omega \Delta\omega T_t \quad , \quad \text{with an error } \leq |\Delta\omega^2 T_z| \quad (9) \end{aligned}$$

where $\vec{T}_z = (\vec{i}_z \cdot \vec{T}) \vec{i}_z$ or the z displacement vector between the tumble accelerometer and the c.g., and $T_t = |\vec{T} - \vec{T}_z| \cdot \vec{i}_t$. Thus, the A_t indicates the value of $\Delta\omega$ under the assumption that $\Delta\omega \ll \omega$.

Since it was felt that this assumption ($\Delta\omega \ll \omega$) would be valid, only the two accelerometers were used (the spin to obtain ω and the tumble to obtain $\Delta\omega$). If this assumption were invalid a third accelerometer, mounted with its sensitive axis parallel to the y-axis, would be needed to give a more accurate indication of the rotation vector. See Appendix B.

The potentiometer-type accelerometer transforms the square of the effective angular velocity, i.e., the effective acceleration, into a resistance value. The varying resistance of the accelerometers is used to linearly control the period of one-shot multivibrators* in the pulse encoding circuits and, hence, the duration of the first and third transmitted pulses.

The dispensing rate is sensed by three small plungers spring-loaded against the side of a dipole disk. As the dipoles dispense, the disk radius is reduced. After sufficient reduction in this radius the dipole disk no longer restrains the plungers; thus, they displace outward, releasing grounding switches. The switching increases the impedance and voltage reference of a parallel resistor network which, in turn, increases the duration of the one-shot MV controlling the duration of the second pulse. The three plungers, spaced at different radial distances, are exposed at three different stages in the dipole dispensing. Thus, the second pulse progresses through four widths, each width indicating an approximate radius in the dipole disk. Ground

* Hereafter the term multivibrator will be designated MV.

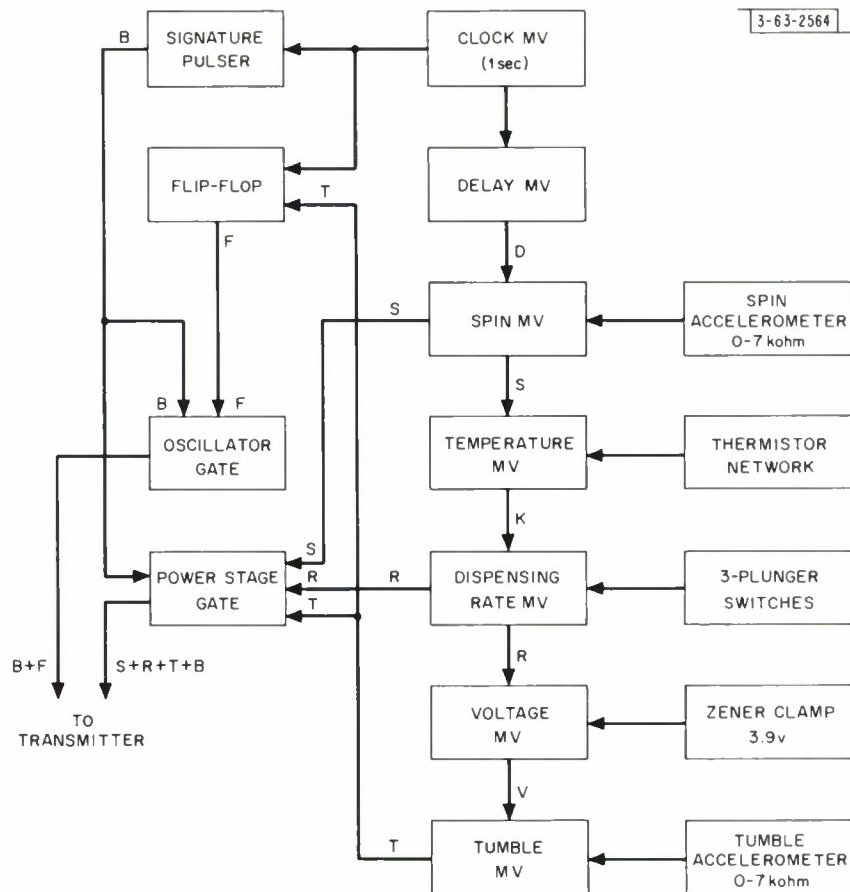


Fig. 6. Logic circuitry functional diagram.

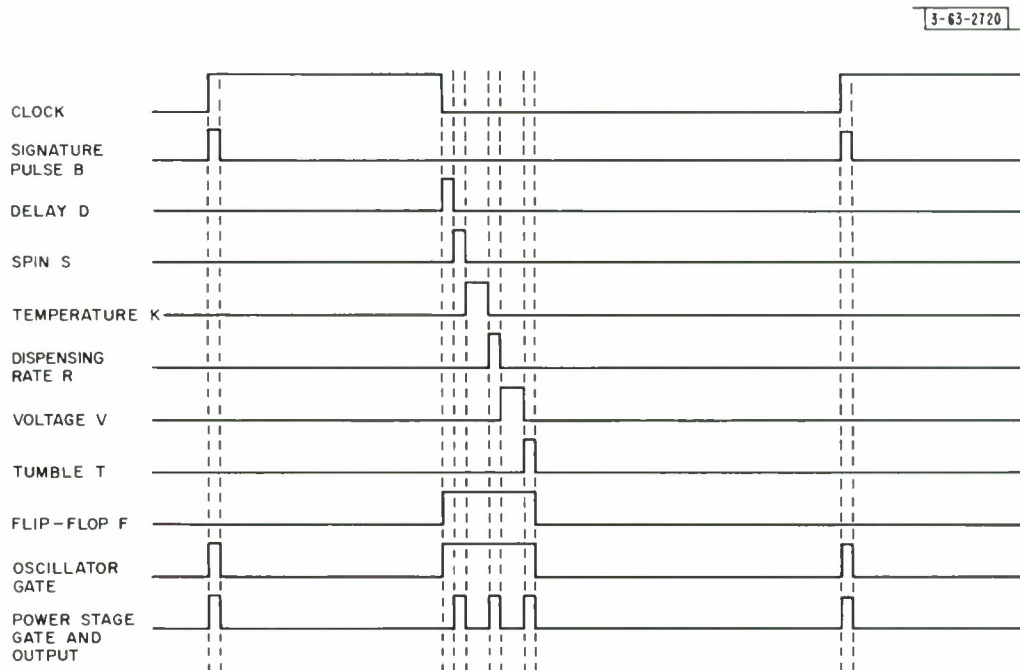


Fig. 7. Logic timing diagram.

switches, not floating switches, were used with the plungers to minimize the number of sealed feedthroughs needed in the package and to maintain simplicity in the circuitry.

System temperature was monitored through the use of a thermistor network. Two thermistors and three resistors yielded a network resistance whose impedance was approximately linear with respect to temperatures from -50° to $+50^{\circ}\text{C}$. The temperature information was assigned to the spacing between the first and second pulses. This was accomplished by utilizing a one-shot MV whose duration was a linear function of the thermistor network resistance.

The space between the second and third pulse was encoded with the logic voltage. This was implemented by forcing a nonsymmetrical-type recovery in a one-shot MV. This circuit will be discussed in detail in the next section.

III. LOGIC CIRCUITRY

A. Functional Design

It is the function of the logic circuitry to sample the sensor outputs, convert these outputs to a form compatible with PDM, and drive the transmitter accordingly. This function is illustrated in the logic diagram (Fig. 6).

The logic circuitry is essentially a one-second, free-running clock MV triggering a chain of six, consecutively triggering, one-shot MVs. The clock MV controls the over-all one-second cycle time. All but the first one-shot MV control pulse widths or pulse spacings. The sequential timing of these MVs is illustrated in the logic timing diagram (Fig. 7). The output of the clock MV C drives the delay MV with its trailing edge. The delay MV output D lasts for about 10 msec and then falls, triggering the spin MV. The spin MV output S triggers the temperature MV with its falling edge. This process continues until all six MVs have been triggered. Thus, outputs D (delay MV output), S (spin MV output), K (temperature MV output), R (dispensing rate MV), V (voltage MV), and T (tumble MV) are consecutive and mutually exclusive. The sum $S + R + T$ forms the logic of the transmitter information output and corresponds to the three transmitted pulses. Outputs K and V show up as the spacings between S and R, and R and T, respectively.

The fall of the complementary output of the clock MV C is used to create a short signature pulse B. The existence of this pulse relies only on the clock MV and has no sensor dependence. This pulse is added to $S + R + T$ to form $S + R + T + B$ and makes up the final transmitter output format. Thus, the existence of the telemetry beacon (the prime concern of the canister) is, by virtue of B, dependent on only 10 percent of the logic circuitry and on none of the sensors. This factor assures maximum operating reliability for the telemetry beacon.

The sum $S + R + T + B$ is formed in a diode network and is used to gate the drive of the power amplifier in the transmitter. This sum could not be used to gate the entire transmitter because the crystal controlled oscillator takes from 5 to 10 msec to frequency stabilize. A stable carrier frequency is necessary to assure accurate pulse-width measurement. On the other hand, to leave the oscillator on continuously would require a prohibitively large amount of power. To allow the oscillator ample time for stabilization without sacrificing power, the oscillator was turned on 10 msec prior to the first pulse and was left on until the fall of the third pulse. This oscillator gating was accomplished by setting a flip-flop with the clock MV C and resetting it with the fall of the tumble MV T. The flip-flop output was, therefore, $F = D + S + K + R + V + T$ with the resulting oscillator stabilization time of D. Pulse B, summed with F in a diode gate,

was also used to gate the oscillator. This resulted in an oscillator gate output equal to $F + B = D + S + N + R + V + T + B$.

Since B contains no information its pulse width does not have to be read accurately. Therefore frequency stabilization is not necessary for the pulse. For this reason (and simplicity) the oscillator was given no stabilization time prior to the transmission of B . The resulting duty cycle of the oscillator was approximately 10 percent.

B. Circuits

Three basic objectives were sought in the design of the logic circuits: low power, simplicity, and high reliability. The MV chain approach, with passive sensors in the timing networks, guaranteed simplicity and reliability while the use of load switching and low-current transistors helped achieve low power. The schematic (Fig. 8) shows the logic circuitry and its encoding of the sensors.

A four-transistor, complementary MV was chosen for the clock. This type of MV affords good triggering outputs and low power drain. Since the power dissipation is dependent on the base resistors rather than collector resistors, a saving in power of somewhat less than $\beta/2$ is realized. The average power dissipation of the clock is approximately $200 \mu w$.

The temperature dependence of the electrolytic capacitors was, to a large extent, compensated for by the variation in temperature of the V_{eb} and V_{ec} of the silicon transistors. Therefore the timing is relatively temperature independent, i.e., the period of the clock did not vary more than a few tenths of 1 percent over the entire temperature range.

The delay, one-shot MV is in part complementary in that only one of its collector resistors is replaced by a complementing transistor. The influencing feature here is the fact that this is a very low duty-cycle MV (less than 1 percent) and, therefore, the one collector resistor dissipates power for only a short time. This modification results in increased reliability, i.e., saves 1 (of 4) transistor and 3 (of 26) solder points. A decrease in complexity and a saving of power is also realized. The power dissipated in this three-transistor MV compared to a two- and four-transistor MV is shown in Appendix C. For a 1-percent duty cycle (10-msec pulse), the relative saving in power is nearly 50 percent.

The period of this MV is, as with most of the other MVs, relatively independent of supply voltage V_+ . This can be seen by noting that during the activation of the MV, the recovery voltage V_b on the base of the off transistor is approximately

$$V_b \approx V_+(1 - e^{-t/\tau})$$

for

$$V_+ \gg V_{eb} \quad . \quad (10)$$

Here, V_+ (the supply voltage) is also the return voltage. The recovery voltage is V_b . The length of this period is approximately determined by the time it takes V_b to reach ground, i.e., the time T_d such that

$$V_+ \left(1 - 2 e^{-T_d/\tau} \right) = 0 \quad . \quad (11)$$

The solution of Eq. (11) is

$$T_d = \tau \ln 2 \quad (12)$$

and is independent of the supply voltage. The only assumption made here is that the supply voltage is large compared to the transistor saturation voltages (V_{eb} and V_{ce}).

The spin MV differs from the delay MV only in the time-constant resistance network. Here, the resistance of the spin-measuring accelerometer is used in conjunction with the timing capacitor to determine the pulse width. A 2-kohm resistor was added in series with the 0- to 10-kohm accelerometer resistance to achieve a 1.2- to 8-msec pulse width. To prevent this low impedance from loading the battery supply, a 100-kohm resistor was switched in series with the timing resistance in the base path when the MV was not in the activated state. This was done by use of a shorting transistor driven from the opposite collector as shown in Fig. 9. A second 100-kohm resistor was put in parallel with the accelerometer to keep malfunctions in the leads or accelerometer from preventing the triggering of the next MV.

The temperature MV also differed from the delay MV only in its timing resistance network. Here, three resistors and two thermistors composed a network whose resistance varied in an approximately linear fashion with temperature over the designed temperature range. A single thermistor network could not provide good resolution over the temperature range -50° to $+50^\circ\text{C}$ because the resistance of a thermistor has, basically, a logarithmic dependence on temperature.

The dispensing-rate MV had both a variable timing impedance and a varying reference return voltage in the timing network. To minimize the number of feedthroughs in the canister cover, each plunger system was assigned but one feedthrough. Thus, the indication of a plunger movement had to be in the form of a breaking of a ground switch. The timing circuit for this system is shown in Fig. 10. Appendix C contains the derivation of the resistance value controlled by the grounding switches used to give the appropriate pulse widths.

The periods of these MVs, as shown in Eq. (11), are effectively independent of supply voltage by virtue of the fact that (see page 9) the recovery voltage V_b in the timing base transistor is linear with the return voltage V_+ . By preventing this linearity, the period of the MV can be made to vary with supply voltage. In the voltage MV, therefore, a Zener was tied to the critical base preventing this base voltage from swinging to its full negative value. The recovery voltage equation then becomes

$$V_{bz} = V_+ - (V_+ + V_z) e^{-t/\tau} \quad (13)$$

for

$$V_z \leq V_+ ,$$

where V_z is the Zener breakdown voltage and V_{bz} is the recovery voltage (in this MV). Note that V_{bz} is not linear with V_+ . Again, assuming that the recovery time (T_v in this MV) is governed by the time it takes V_{bz} to reach ground,

$$V_{bz}(t) = V_{bz}(T_v) = 0 = V_+(1 - e^{-t/\tau}) - V_z e^{-T_v/\tau} , \quad (14)$$

or

$$T_v = \tau \ln \left(\frac{V_+}{V_+ + V_z} \right) \quad (15)$$

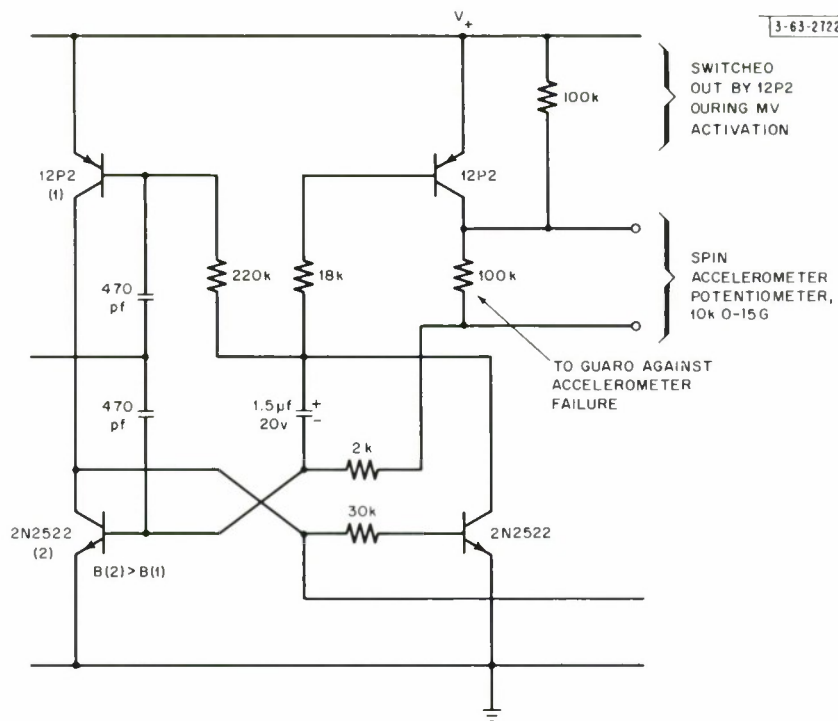


Fig. 9. Spin and tumble multivibrator.

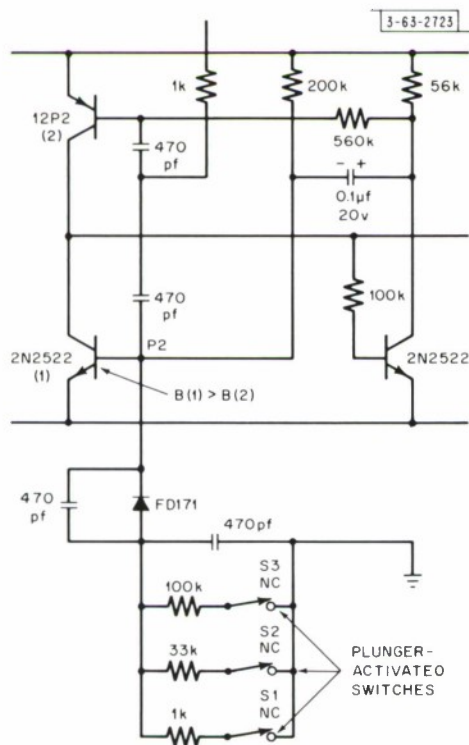


Fig. 10. Dispensing-rate multivibrator.

which has a strong nonlinear dependence on V_+ . The change in T_v with respect to V_+ is given by Eq. (16), i.e.,

$$\frac{\partial T_v}{\partial V_+} = \frac{\tau}{V_+ \left(1 + \frac{V_+}{V_z}\right)},$$

for

$$V_z \leq V_+ \quad (16)$$

Since $\partial T_v / \partial V_+$ increases monotonically with respect to V_z , it is desirable to make V_z as large as possible for maximum sensitivity. However, the condition for voltage dependence is governed by $V_z < V_+$ and, therefore, V_z should not exceed the V_+ minimum that would be of interest. For V_+ of 6 volts, a V_z of 3.9 was selected.

The tumble MV is identical to the spin MV with the tumble accelerometer controlling the timing resistance. The trailing edge of output of this last MV resets the flip-flop. The signature pulse is obtained through a one-transistor slicer gate. The transmitter and oscillator gate is a diode network feeding two double-transistor switches. Figure 11 is a photograph of the logic card before potting.

IV. TELEMETRY TRANSMITTER

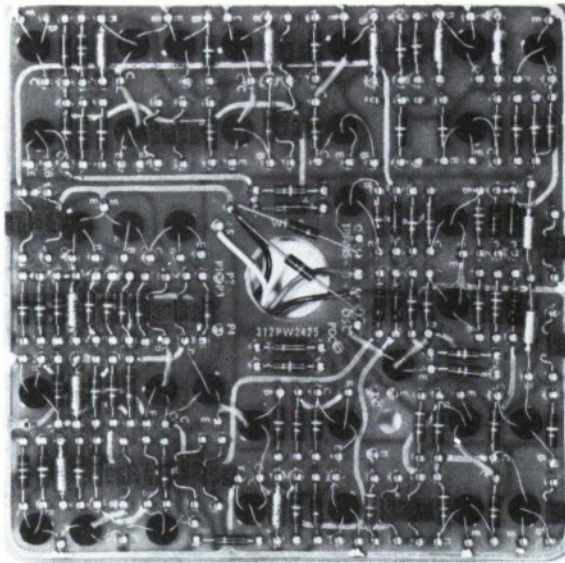
The primary function of the transmitter is to provide a signal for accurate ground-based tracking. Therefore, a crystal-controlled transmitter frequency is mandatory. The PDM modulation system readily permits the use of a crystal-controlled carrier frequency, since the logic gate circuits merely vary the duration of pulses and not their frequency. The system response in the frequency domain is nearly a line spectrum because the pulse widths are long compared to an RF cycle. Since the peak signal-to-noise ratio is high (and the frequency spectrum is narrow band), ground detection of the signal is simplified and the beacon track function enhanced.

The transmitter is of conventional design. The most important circuit design objectives were efficiency, reliability, and small size because of the limitations imposed by the mechanical canister design and system life requirements. The all-solid-state approach is mandatory since vacuum tubes are large, are disturbed by vibration, and require complex power converters.

Figure 12 is a block diagram of the transmitter. Figure 13 is a photograph of a flight transmitter ready for final potting and assembly. The transmitter has four basic circuits:

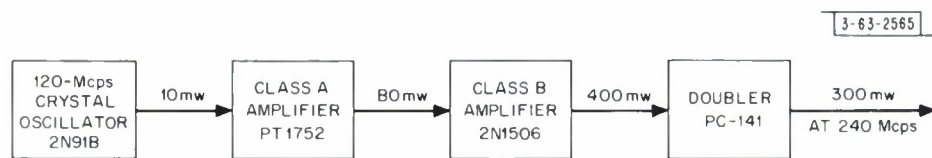
- Low-power crystal oscillator
- Class A driver
- Class B power amplifier
- Varactor frequency multiplier output stage.

Frequency stability is a common problem encountered in transmitter design. Circuit and device parameter drift caused by time, temperature, applied voltage, or load conditions may result in slight changes in the frequency of oscillation. A high Q quartz crystal was used in the base circuit of the oscillator to stabilize the frequency. The power dissipation ability and the stability of the crystal provided an upper limit to the power consumption of the oscillator.



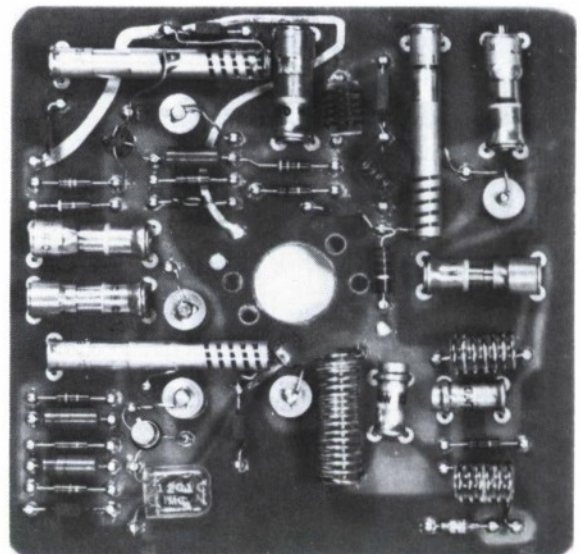
PT40-694

Fig. 11. West Ford telemetry canister before potting.



3-63-2565

Fig. 12. Transmitter block diagram.



PT40-669

Fig. 13. Flight transmitter before potting.

Since efficiency of the oscillator increases with output level, it was desirable to operate near the upper limit. In addition, oscillator power output was high enough to preclude an additional stage of amplification to meet transmitter-power output requirements.

Since oscillator design involved so many compromises, an experimental approach was used to obtain the desired performance. Figure 14 is the temperature-frequency stability curve for a typical battery-powered circuit in a pulsed mode. As the figure indicates, stability under these conditions was good. The reduction in device gain and the increase in battery impedance at low temperatures proved to be the most difficult problems to overcome. They were solved throughout the transmitter by experimentally optimizing each component value, then each circuit and, finally, the entire transmitter (as a function of temperature and applied voltage). The oscillator is controlled, by a separate gate, from the logic circuits. The gate turns the oscillator on approximately 5 msec before the chain of data pulses to permit transmitter-frequency stabilization. The oscillator remains on during the entire period of data transmission. Because of the pulsing of the class A driver, the oscillator drives a varying load which in turn effects oscillator stability. Due to the relatively large ratio of oscillator output impedance to driver output impedance, this effect did not degrade transmitter performance.

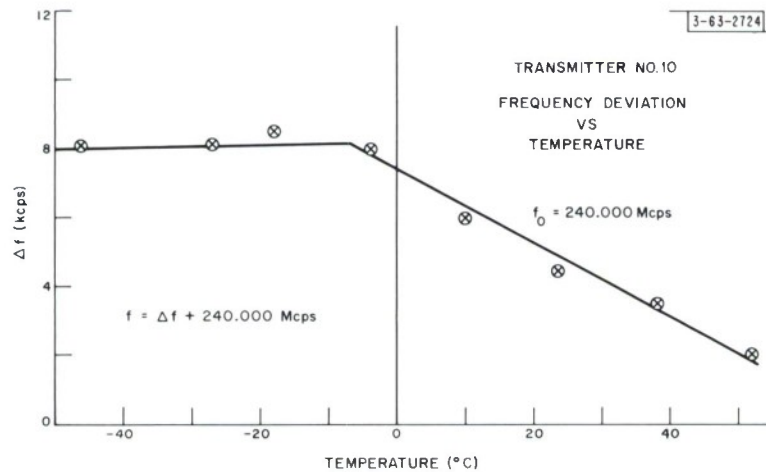


Fig. 14. Temperature-frequency stability.

The class A stage operates at 25-percent efficiency with a gain of 9 db. Power output is 80 mw. A bias voltage obtained at the collector of the class A stage is used to provide base bias of the class B power amplifier. In this way, bias power is conserved. By using experimentally found optimum resistor values in the voltage divider network, nearly constant output power may be obtained over the temperature range -50° to $+50^{\circ}\text{C}$. The class B amplifier is pulsed by the power from the driver rather than by a separate gate. The power stage has a collector efficiency of 31 percent.

The varactor multiplier operates at 75 percent efficiency. The multiplier stage is of slightly unusual design, but has the advantage of additional output waveform filtering. The output section of the multiplier contains a parallel resonant trap for the fundamental frequency. However, the circuit values L and C_1 , as shown in Fig. 15, are chosen to series resonate the output circuit at twice the fundamental frequency. The input circuit contains a parallel resonant trap for the output frequency, and the circuit values L and C_2 are chosen for series resonance at the fundamental frequency.

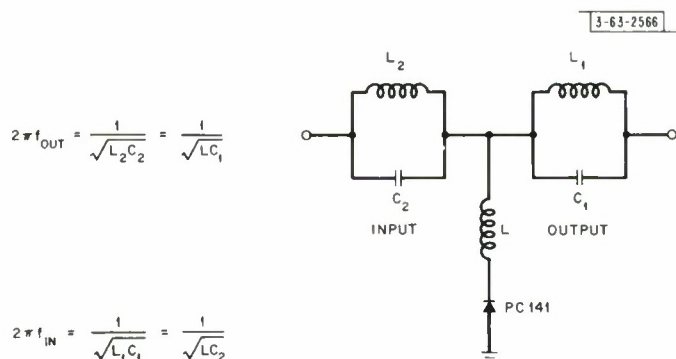


Fig. 15. Frequency doubler circuit.

Total transmitter power drain is 1.8 watts and the output power to the antenna is 300 mw – for an over-all efficiency of 16 percent. At low temperatures (-50°C) power output is 4 db down.

The transmitter output is fed to an antenna system of nominal (50-ohm) impedance. During the first twenty minutes after ejection from the launch vehicle the antenna impedance is almost a short circuit. Experiments indicated that this effect would not damage the transmitter. This was later verified during the actual flight.

The entire transmitter circuit, as shown schematically in Fig. 16, is constructed on one printed-circuit card approximately 4 inches square. Considerable difficulty was experienced with the printed-circuit board approach due to ground currents, coupling between the closely spaced elements, and parasitic circuit values of the printed wiring. These difficulties were overcome through a stage-by-stage layout of the transmitter circuit, as opposed to a complete testing of the circuit layouts.

After the components were mounted on the printed-circuit board, the transmitter was potted in a high-temperature foam material. The common epoxy materials have high RF dissipation factors which result in greatly reduced Q's of RF components (notably, inductances) and in any component where the RF fields tend to be strong near the surface of the component. On the other hand, the low-density, high-temperature, foam potting material has a low dissipation factor and makes an excellent RF encapsulating material.

Many interference (false triggering of the logic) problems were encountered on some of the early engineering models of the telemetry gear. They were due to: the low power level of the logic circuits, the high parasitic RF fields of the transmitter, and the close coupling (both physical and electrical) between the logic and transmitter.

The difficulty was overcome by using more RF isolation between the logic and the transmitter and by using RF chokes and bypass capacitors in the wiring between the logic card and transmitter. The radiation pickup caused by the proximity of RF circuits to the digital circuits was reduced by completely enclosing the potted transmitter in a grounded metal container. Thus, the only radiation from the transmitter to the logic was that by leakage coupled by the connecting output and input wires.

V. TELEMETRY ANTENNA AND MATCHING NETWORK

The antenna for the telemetry package consists of a set of four unfurlable monopoles fed in progressive phase quadrature. Electrically, it is nearly equivalent to the well-known turnstile antenna* (named for its mechanical resemblance to a turnstile). The spatial radiation pattern

*G.H. Brown, *Electronics* 9, 14 (1936).

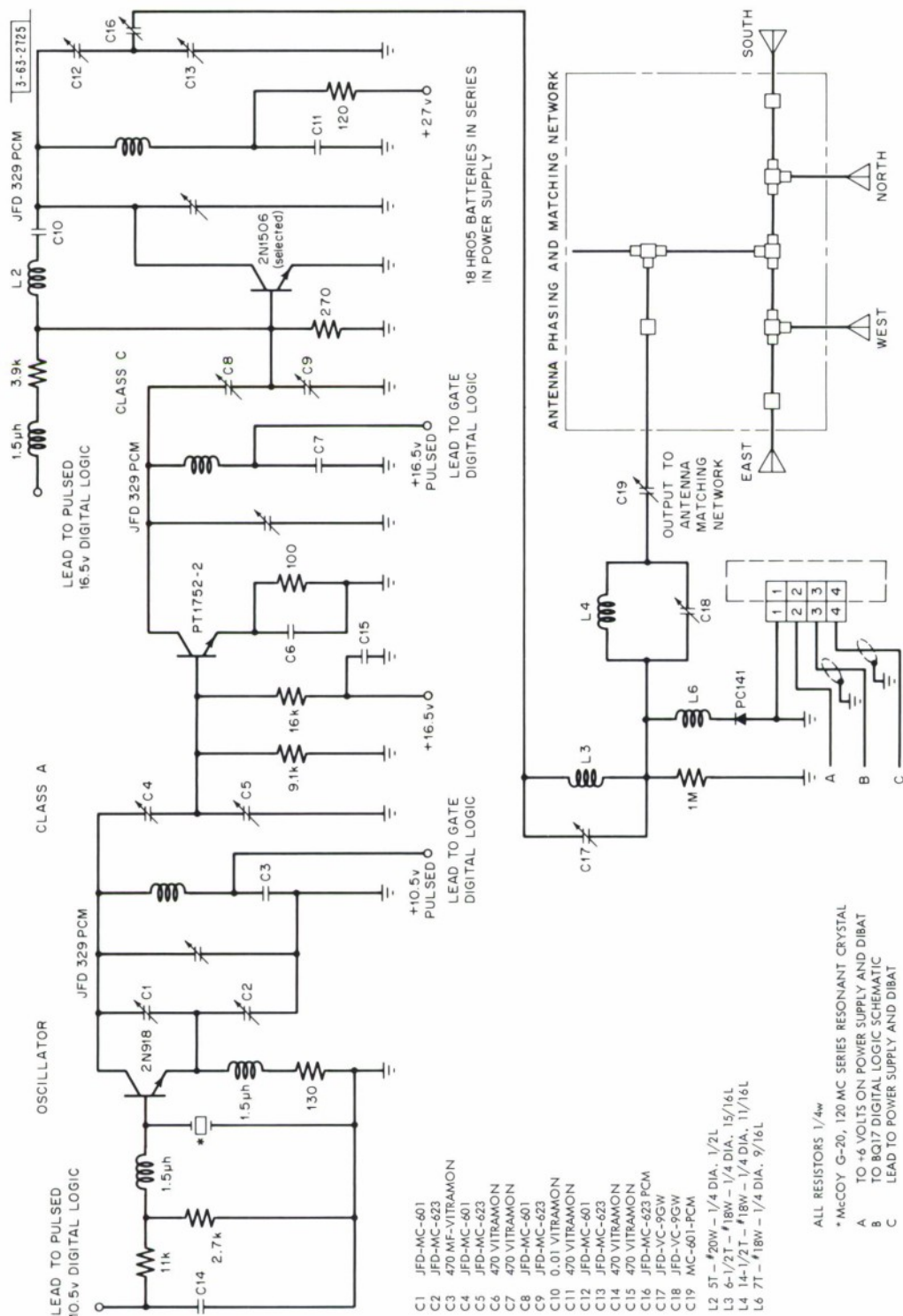


Fig. 16. Transmitter and antenna schematic.

of a turnstile is reasonably omnidirectional, the total variation in the power pattern being less than 5 db (depending on the length of the dipoles). For this reason, approximations to the turnstile have found wide use as satellite telemetry antennas. The pattern about the axis is four-way symmetric with a max-to-min ratio of less than 2 db.

The reason for using unfurlable radiators of any kind is that the package is electrically small, about one-tenth wavelength in linear dimensions. Electrically, small antennas have a highly reactive input impedance and are, therefore, hard to match. It was expected that the matching network for a fixed antenna would either be too bulky for the package or too lossy, considering the low transmitter power. Once an unfurlable type was permitted, it seemed logical to go to the four monopoles which, before and after unfurling, have a maximum moment of inertia about the desired spin axis of the package and a symmetric radiation pattern.

A. Electrical Design

Figure 17 is a sketch of the telemetry package showing the four monopoles unfurled. They emerge from the canister 60° from normal so that they can be easily wrapped around the canister when furled. The curvature of the monopoles is caused by the centrifugal force of rotation. The monopoles are mechanically held by end seals passing through the canister walls. The end seals mate with micro-miniature coaxial connectors inside the canister. The phasing and matching network for the monopoles consists of micro-miniature coaxial cables and connectors which fit into an odd-shaped small space available for the network.

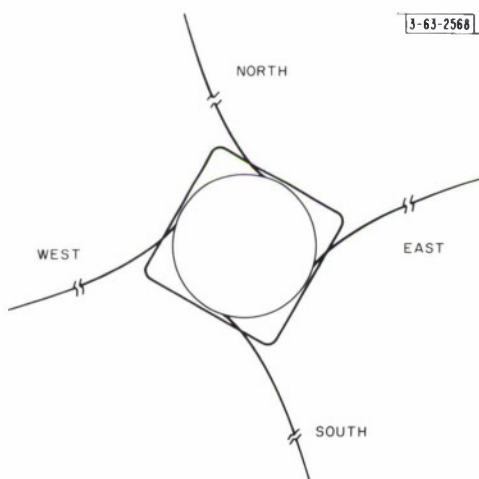


Fig. 17. Telemetry canister showing four monopoles unfurled.

How the monopoles (labeled, consecutively, North, East, South, and West) are fed in progressive phase quadrature will now be explained.

North and South, as a pair, can be fed in phase opposition by connecting North through a coaxial line of any length l to a Tee adapter and South through a similar line of length $l + \text{one-half wavelength}$ to the Tee. To obtain the 180° relative phasing and equal amplitude, North and South must be identical and the cables must be nearly lossless and different in length by one-half wavelength. The Tee was connected directly to the North end seal in the model built. Likewise, East and West are fed in phase opposition, the Tee adapter being connected to the

West end seal. When the remaining terminals on the North and West Tees are excited with equal amplitude and phase quadrature signals, the four monopoles will then be fed in progressive phase quadrature as desired.

A straightforward way to excite two equal loads in phase quadrature is to match and connect them to two phasing cables of like Z_0 but of different lengths (L and $L + \text{one-quarter wavelength}$). Then the cable inputs are fed in parallel. The common input terminal (the input to a Tee adapter) can be matched to 50 ohms by use of a line stretcher and stub. Figure 18 shows the total network, including the phase opposition lines for the North-South pair and East-West pair. Instead of matching the North-South and East-West pairs to the characteristic impedance of the phasing cables, it is possible to modify the lengths of the phasing cables. That is, for any two equal decoupled loads there exist pairs of lengths ℓ_1 and ℓ_2 for two phasing cables fed in parallel so that the loads are fed with equal amplitude, phase quadrature signals. Here the two equal decoupled loads are the North-South pair and the East-West pair. The cable lengths are given by simultaneous solution of Eqs. (17) and (18) for $\beta\ell_1$ and $\beta\ell_2$:

$$r^2 \cos^2 \beta\ell_2 + (x \cos \beta\ell_2 + \sin \beta\ell_2)^2 = r^2 \cos^2 \beta\ell_1 + (x \cos \beta\ell_1 + \sin \beta\ell_1)^2, \quad (17)$$

and

$$\frac{x \cos \beta\ell_2 + \sin \beta\ell_2}{r \cos \beta\ell_2} = - \frac{r \cos \beta\ell_1}{x \cos \beta\ell_1 + \sin \beta\ell_1}, \quad (18)$$

where

r = load resistance normalized to the cable characteristic impedance,

x = normalized load reactance,

$\beta\ell_1, \beta\ell_2$ = electrical length of phasing cables.

Equations (17) and (18) are derived in Appendix D. As an alternative to solving Eqs. (17) and (18), one can break the problem into two parts. Find the length L of a cable whose input impedance Z_i is pure resistance when the cable is terminated in Z . Then, letting $r = r_i$ and $x = 0$ in Eqs. (17) and (18), we have

$$r_i^2 \cos^2 \beta\ell'_2 + \sin^2 \beta\ell'_2 = r_i^2 \cos^2 \beta\ell'_1 + \sin^2 \beta\ell'_1 \quad (19)$$

$$\tan \beta\ell'_1 \tan \beta\ell'_2 = -r_i^2. \quad (20)$$

Equations (19) and (20) are satisfied by

$$\tan \beta\ell'_1 = \pm r_i; \quad \tan \beta\ell'_2 = \mp r_i \quad (21a-b)$$

then

$$\ell_1 \text{ in Eqs. (17) and (18)} = L + \ell'_1 \text{ in Eq. (21a)}$$

and

$$\ell_2 \text{ in Eqs. (17) and (18)} = L + \ell'_2 \text{ in Eq. (21b)}.$$

These two phasing cables are then connected to the phasing Tee adaptor whose input impedance is matched to 50 ohms, as before. This network, shown schematically in Fig. 19, was the one used.

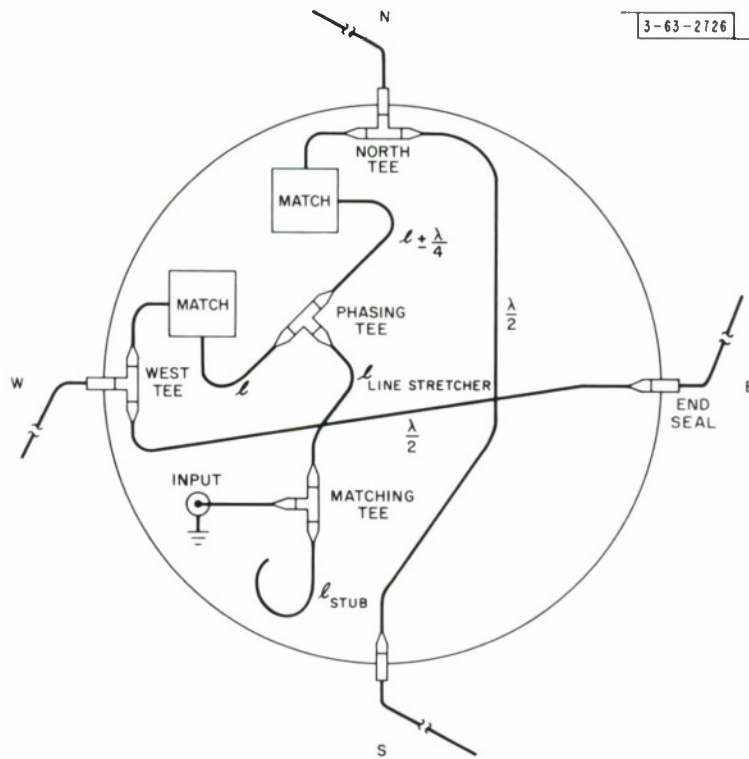


Fig. 18. "Conventional" phasing and matching network for telemetry antenna.

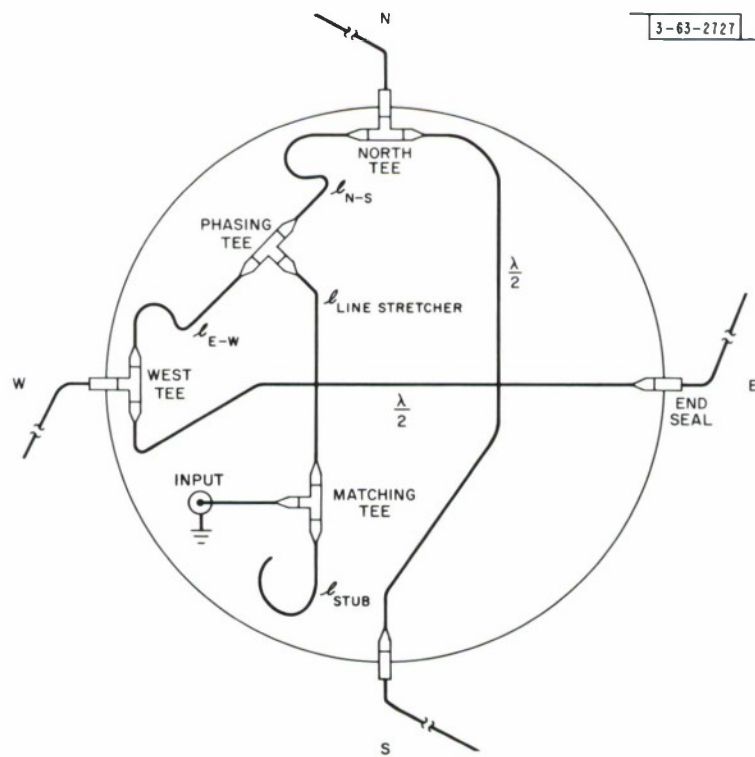


Fig. 19. Phasing and matching network for telemetry antenna.

B. Experimental Adjustment of Variables

The design variables available for the telemetry antenna, including its phasing and matching network, are:

- Length of the monopoles
- Lengths of phasing cables ℓ_1 and ℓ_2
- Cable lengths for the matching network.

The objectives of the electrical design are a radiation pattern in the plane of the monopoles (which is four-way symmetric) and a 50-ohm input impedance to the matching network. The matching network has no effect on the shape of the radiation pattern, but the lengths of the monopoles and phasing cables affect the matching network required. Therefore, the lengths of the monopoles and phasing cables are adjusted before the matching network is made. The coaxial cable used is RG-188 and the connectors are micro-miniature (of a type made by Amphenol Corp., Sealectro Corp., and Micon Electronics, Inc.).

Since it was desirable to fix the monopole lengths before the canisters were fabricated, impedance and radiation pattern measurements were made on a breadboard model of the payload. The breadboard was a box made of sheet brass having nearly the same outside shape as the canister. The monopoles were thin wires soldered to the pins of coaxial bulkhead receptacles which then approximated the end seals used in the actual canister. Figure 19 is a schematic of the breadboard (as well as for the payload) with this approximation. The monopoles are curved by the centrifugal force of rotation, since they emerge from the canister at an angle of 60° off normal. A canister with monopoles was photographed while rotating in a vacuum chamber so that the shape of the curve could be determined. For impedance and pattern measurements, the monopoles were held to this curved shape by taping them to a block of styrofoam. The steps in finding the lengths of the monopoles and various phasing and matching lines were as follows. Half-wavelength cables were made for feeding the East-West and North-South pairs, respectively, in phase opposition. The input impedance of the North-South pair fed out of phase was measured at the North Tee as a function of monopole length. A length of $11\frac{1}{2}$ inches gave about 20 ohms impedance. Lengths of the phasing cables ℓ_{N-S} and ℓ_{E-W} were calculated. A number of cables were made of slightly differing lengths (including the calculated lengths) for both ℓ_{N-S} and ℓ_{E-W} .

Then the azimuth pattern (in the plane of the monopoles) was measured for four monopoles. The length of the monopoles was varied, and slightly different length phasing cables were tried. The tentative lengths of the monopoles ($11\frac{1}{2}$ inches) and phasing cables selected were those giving the most nearly symmetric pattern.

These tentative lengths were then used on a payload canister, when one became available, and rechecked by measuring azimuth patterns as before. Again, slightly different length phasing cables were tried. Also, the monopoles were shortened to $11\frac{1}{4}$ inches. The final measured azimuth patterns for the two payload canisters which flew are shown in Figs. 20 and 21. After suitable radiation patterns were obtained, coaxial matching networks (consisting of a line stretcher and open-circuited stub) were made of micro-miniature parts.

The length of the monopoles and the phasing and matching lines for the same two payload canisters are given in Table I. Coaxial connectors on the cables are Amphenol, types 27-7 and 27-8. The Tee adaptors are Sealectro micro-miniature Con-Hex type. The cable is RG-188.

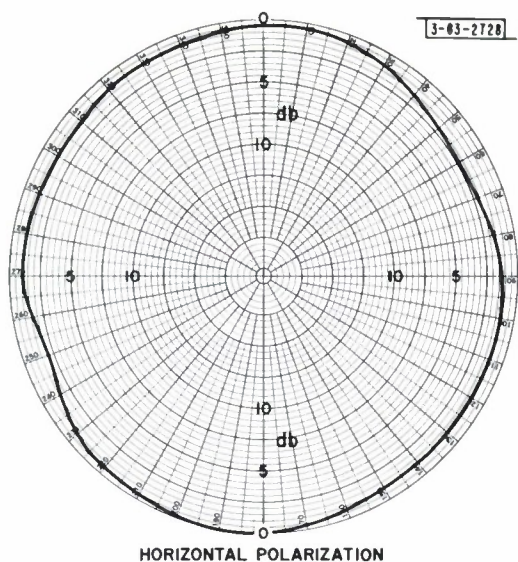


Fig. 20. Azimuth pattern of Model No. 4 at 240 Mcps.

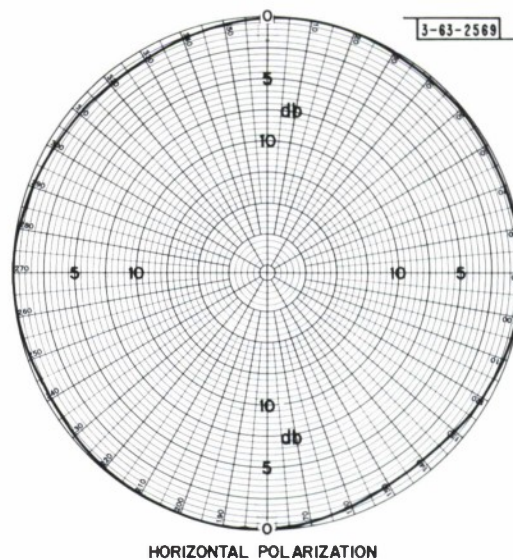


Fig. 21. Azimuth pattern of Model No. 5 at 240 Mcps.

TABLE I LENGTHS OF MONOPOLES AND PHASING AND MATCHING LINES*		
	Model No. 4	Model No. 5
Monopole lengths		
$\lambda/2$ cable	11-1/4	11-1/4
$\lambda/2$ cable	17-7/16	17-7/16
Phasing cables		
ℓ_{N-S}	14-1/2	19-3/8
ℓ_{E-W}	18-7/8	15-1/8
Matching network		
$\ell_{\text{line stretcher}}$	2-1/4	2-1/4
$\ell_{\text{oc stub}}$	4-1/8	4-5/16
*Measured in inches.		

C. Performance

Azimuth patterns of the two payload models at 240 Mcps are shown in Figs. 20 and 21. The total variation between E_{\max} and E_{\min} was $2\frac{1}{2}$ db for model No. 4 and about 1 db for model No. 5. Azimuth patterns were measured at 240 ± 5 Mcps and ± 10 Mcps for No. 5. The variations between E_{\max} and E_{\min} as a function of frequency are as follows:

Frequency (Mcps)	230	235	240	245	250
Azimuth pattern variation (db)	$7\frac{1}{2}$	$3\frac{1}{2}$	1	$3\frac{1}{2}$	$5\frac{1}{2}$

The input VSWR's referred to 50 ohms at 240 Mcps were 1.1 for model No. 4 and 1.0 for model No. 5.

The gain of a prototype model telemetry antenna was compared with a matched half-wave dipole radiating maximum signal toward a detector. The dipole gave 3.3 db more signal at the detector. This is very nearly as expected because the power in the telemetry antenna is evenly divided between the two decoupled pairs of monopoles. In a turnstile antenna (to which the telemetry antenna is nearly equivalent) it can be shown that if one dipole radiates maximum signal toward a detector, the other dipole has a null toward the detector.

The final electrical test involving the telemetry antenna measured the radiated power from the package. Figure 22 is a schematic of the circuit. The radiated power was measured by comparing it with the radiation from a matched dipole with a known input power. The signal levels received at the corner reflector were compared by a precalibrated, padded crystal mixer and oscilloscope instead of a meter because the telemetry signal was pulsed.

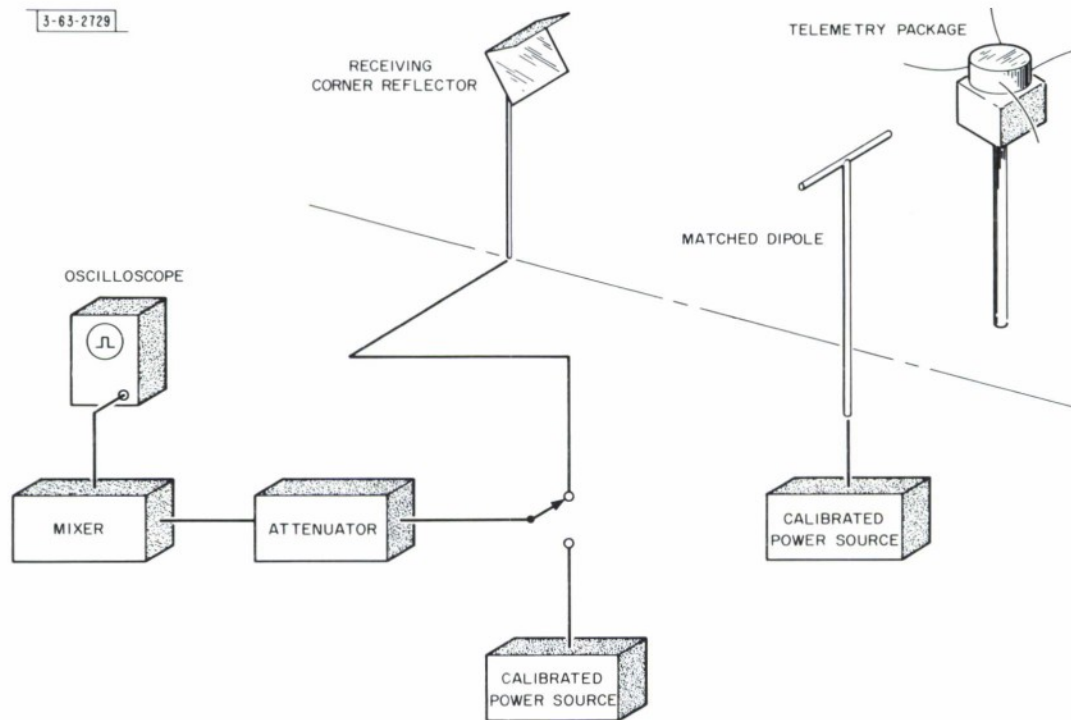


Fig. 22. Range for measuring telemetry radiated power.

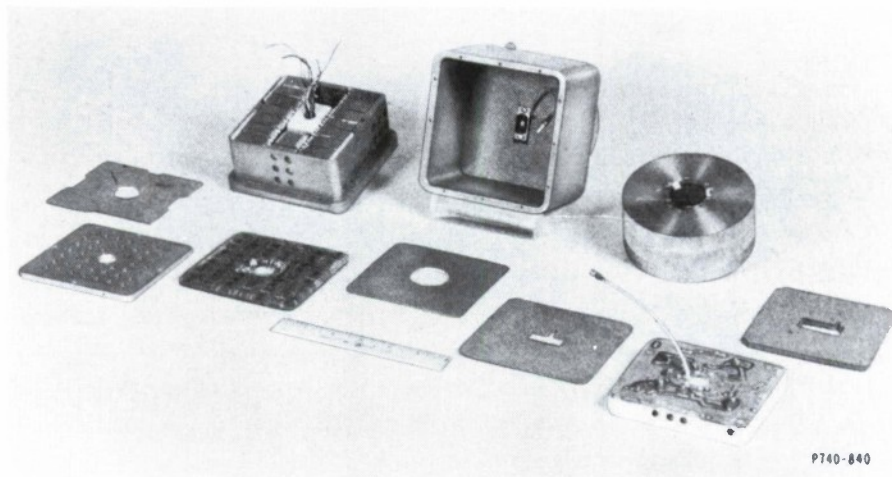


Fig. 23. West Ford telemetry canister disassembled.

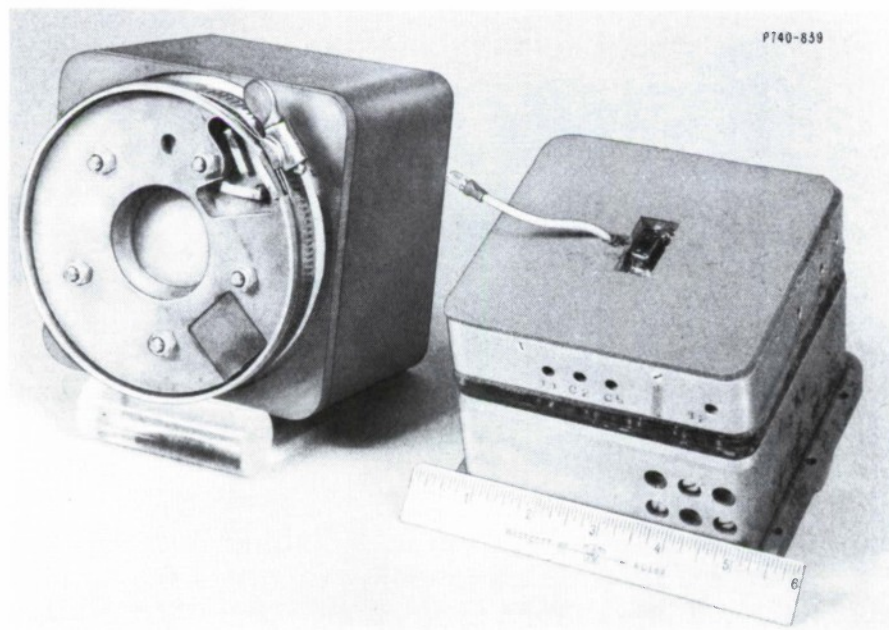


Fig. 24. Canister ready for cover mounting.

The distance from the transmitting antenna to the corner reflector was about 20 feet over smooth ground, the height of all antennas being about 9 feet. The radiation test was performed many times for different packages and as a function of temperature. In all tests, the range from package to corner reflector was identical to the range from dipole to corner reflector. The radiated power of the orbited payloads was satisfactory.

VI. MECHANICAL

Figures 23 and 24 illustrate the canister mechanical design and assembly. Each basic member, logic, transmitter, etc., occupies a layer stacked one upon another. The first layer contains the accelerometers and battery pack housing; the second, logic circuitry; the third, the transmitter; and the fourth, the antenna-matching network. These layers are enclosed by a steel cover on which are mounted the turn-on switch, antennas, and dispensing rate plungers.

Eighteen Yardney HR05 cells are strapped together to form the main battery supply for the transmitter. Fourteen Yardney HR01 cells, in two parallel combinations of 7 each, comprise the power supply for the 120-Mcps oscillator. The logic derives its power from the remaining four HR05's in the battery pack. The two accelerometers are fitted into the battery pack with the sensitive axis of the spin accelerometer perpendicular to the z-axis and the sensitive axis of the tumble axis parallel to the z-axis.

The distribution board is in the middle of this housing. The RF isolation filters and diodes are mounted on it for battery protection. The batteries can be charged and monitored externally by feedthroughs in series with protecting diodes.

This housing is covered by an insulating card and a metal shield on top of which sits the logic board (Fig. 23). All interconnecting wires run through the middle of the layers (see Fig. 25). The transmitter, enclosed in a metal container, is mounted next (above the logic board). This layer is electrically connected to the above layers by means of a small Cannon connector (for ease in mechanical assembly). See Fig. 25.

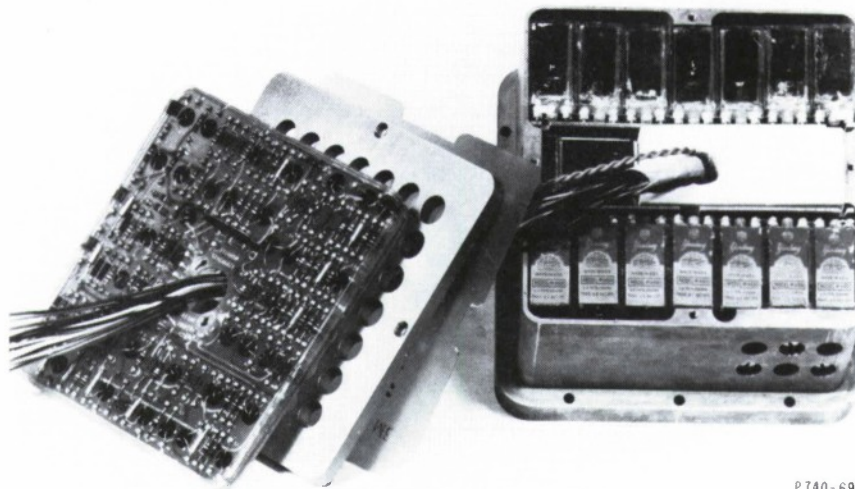
The antenna-matching network feeding the four antenna elements is coiled under the canister cover above the transmitter area. The cover contains the antenna elements, the three plunger assemblies, and a logic turn-on switch activated by the canister's ejection.

The two dipole decks which are to be studied are mounted on top of the canister, depressing the three sublimation plungers (Fig. 3).

The antenna elements are wrapped around the canister in grooves and held in place with naphthalene. In this way, the antenna will not erect until the naphthalene sublimates, i.e., well after canister ejection. This protects the antenna elements during ejection, assembly, and handling.

The canister cover slides over the layers and fits against a flange on the battery housing (Fig. 24). An o-ring provides the seal necessary to maintain internal atmospheric pressure. An internal pressure greater than a few pounds per square inch is mandatory to prevent the battery electrolyte from boiling.

The battery charging feedthroughs in the battery housing base, antenna feedthroughs, turn-on switch feedthroughs, and plunger feedthroughs are all hermetically sealed to prevent air from leaking out. Five screws which connect the canister to the rest of the West Ford dipole dispenser are also sealed with o-rings, providing a complete seal for the canister.



P740-693

Fig. 25. Battery housing and logic board.

VII. RESULTS

Both the square canister and the modified square canister (Appendix B) were placed into successful orbits and telemetered performance data to the West Ford terminals. The round canister was not ejected and, hence, no data were transmitted from this system.

The square canister monitored the dipole dispensing and performance of the West Ford experiment conducted in May 1963. Received data were obtained for $5\frac{1}{2}$ days after ejection — during revolutions 8 through 55. A sample of the quick-look data readout is shown in Fig. 26. Figures 27(a) and (b) show a plot of the measured functions of spin, tumble, dipole dispensation, voltage, and temperature vs time after ejection.

The observed temperature started low ($+3^{\circ}\text{C}$) and climbed to an average of about $+13^{\circ}\text{C}$ after the first 24 hours. After this warming-up period the highest temperature observed was $+16^{\circ}\text{C}$, the lowest was $+10^{\circ}\text{C}$. The high of 16°C corresponds to end-of-day temperature; whereas the $+10^{\circ}\text{C}$ seems to be the lowest night temperature. Revolution 55 demonstrates this temperature correspondence quite clearly in that the canister temperature was $+16^{\circ}\text{C}$ as it entered the earth shadow (night) and $+10^{\circ}\text{C}$ as it left the shadow (day).

The voltage readings fluctuated a few tenths of a volt around 6.2, depending upon the temperature. There was a positive temperature dependence, as expected. A plot of the voltage at 10°C vs time shows that the voltage was slowly dropping off.

The dipole dispensation did not indicate a change until the canister and disks warmed up (for the first two days). The displacement of the third dipole plunger was not observed during the life of the canister.

The values of spin were surprisingly low, i.e., they ranged from 0 to 90 rpm instead of the predicted 400. The tumble accelerometer had an average value of about 50 rpm, which was above the predicted value.

One explanation was that the rotational vector did not line up with the z-axis, but converted to an orientation which reduced both the spin and tumble accelerometer readings. The data received from the modified square canister (see Appendix B) confirmed that an axis conversion

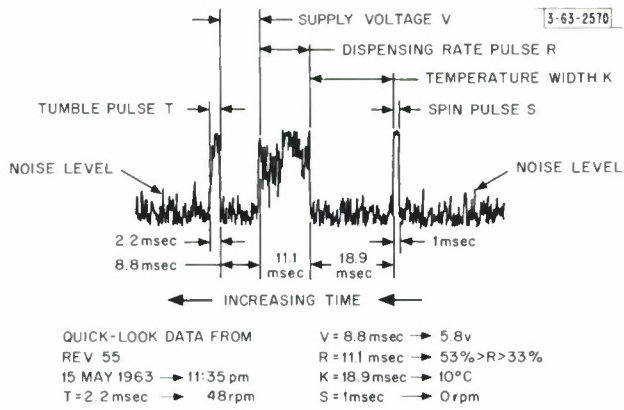
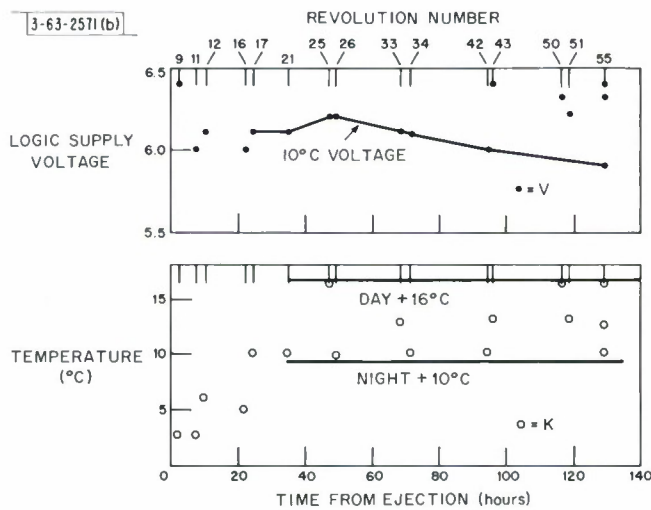
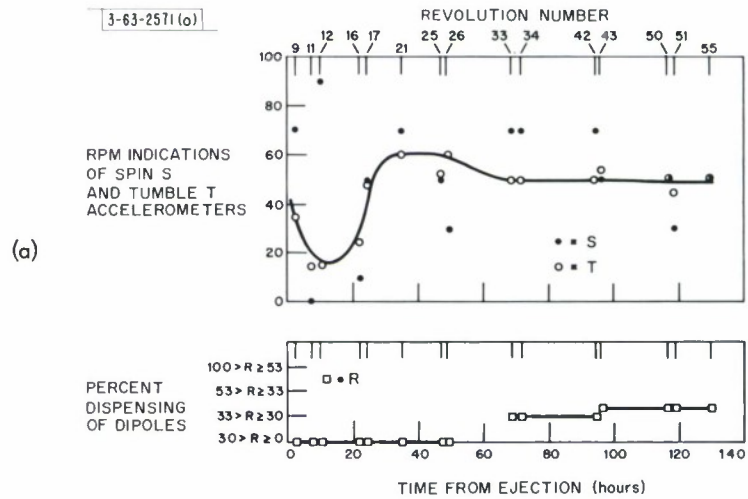


Fig. 26. West Ford telemetry data showing three information pulses.



(b)

Fig. 27. Plottings of canister telemetry vs time.

did occur. However, the spin reading was initially very high in the modified canister; whereas it was not initially high in the first square canister. Also, at no time in the modified square canister did the value of spin drop below 100 rpm.

Subsequent laboratory tests investigating the mechanical stability of the telemetry canister indicated that the maximum moment of inertia of the canister was not about the spin axis of symmetry and that the canister was only marginally stable. Since the cross section of the canister is square, the axis of maximum moment of inertia is not unique. The square canister and the modified square canister were not exact mechanical duplicates and therefore did not have identical stable axes. The accelerometer indications of the various canisters should be quite different, depending upon the location of the stable axis, because of marginal stability and these slight asymmetries.

The lifetime of $5\frac{1}{2}$ days for the first square canister was less than expected even though it was near the one-week-minimum life design time. The system safety factor of four and the conservative battery energy rating implied that a system lifetime of several weeks should have been observed. A possible factor in the degradation of system life was prolonged launch hold which degraded the energy stored in the batteries. The possible existence of a small canister leak permitting, eventually, battery electrolyte evaporation could account for the shortened life.

The dipole-dispensing circuit was not required in the modified square canister, since no dipoles were included in this payload. The dispensing measurement was replaced by the third rotation sensor which checked the rotation axis conversion theory.

Additional batteries were also included in this payload, and the duty cycle was reduced to increase expected system life. The telemetry system functioned properly for 20 weeks in orbit.

ACKNOWLEDGMENT

The authors wish to express their sincere appreciation to Richard H. Baker for his stimulating advice, criticism, and guidance.

In addition, the authors wish to acknowledge the contributions of the following personnel: C. L. Gillaspie, Group 33; R. J. Burns, Group 61; J. H. D. Doucet, E. E. Gaiser, E. Jahnsan, W. F. McBride, G. V. O'Malley, and D. Quintal, Group 63; D. Pantalea and G. F. Raehlk, Group 71.

APPENDIX A

ROUND CANISTER

The round canister was the first proposed and built to monitor a dipole dispenser. This canister differed from the square canister in mechanical design, dispensing-rate sensing, and antenna system.

Integration of this canister with the dipole dispenser dictated that it be round, have an end-mounted antenna, a $\frac{3}{4}$ -inch hole through the middle, and be compatible with an existing dispenser. The assembly of the layers was reversed. The transmitter was mounted on the base plate, was followed by the logic, with the battery pack and accelerometers mounted on top.

All dipole disks were attached to the canister. This resulted in a total integrated length of about 2 feet. An aluminum disk was mounted by a teflon ring $1\frac{1}{2}$ inches off the base of the canister. The transmitter drove the disk against the canister-dispenser assembly producing a dipole radiation pattern. This type of antenna had very low input impedance (5 ohms).

Four optical switches, mounted at different radial distances behind small cover-sealed windows in the canister cover, monitored the state of dipole dispensing. When the sublimation of the dipoles reached a window, reflected and direct light triggered the optical switch behind the window which, in turn, controlled the width of the middle output pulse.

An electrically driven vibrator mounted between the base plate and the antenna was added to aid dipole dispensing.

APPENDIX B

MODIFIED SQUARE CANISTER

A second "square" canister, similar in design to the original "square" canister except for the changes outlined below, was constructed and launched to check the theory that a spin-axis conversion had occurred during the May 1963 shot. A second design objective was a very-long-life system (of the order of 3 months). The system temperatures and voltages were known from theoretical calculations. The data from a long-life system would not only provide a check on these calculations but would also yield significant system reliability information.

Since no dipoles were included in this payload, the space occupied by the two dipole decks (see Fig. 2) was used for additional batteries. In addition, the dipole-dispensing circuit was no longer required. In its place was a third accelerometer, called the axis accelerometer. This accelerometer was added because the assumption made in the sensor section of this report $[(\Delta\omega)\omega]$ was not accurate, i.e., the rotational axis did not approximately correspond to the z-axis. From the three independent accelerometer readings, enough information was obtained to calculate the rotational motion of the canister and to obtain a check on the spin-axis conversion theory.

In the first "square" canister, the entire logic operated in a continuous mode. To increase expected system life a power-control circuit turning off most of the logic circuits during the period of no data transmission was added to the modified system. In the modified system the only circuit that dissipates power continuously is the master clock oscillator and associated delay and signature circuits. The period of the clock was adjusted so that a pulse train occurred once every 10 seconds rather than once every second. The power consumption of these circuits was reduced by the use of higher coupling resistance values. In the long-life system the signature pulse is generated but not transmitted. Instead, it is used to trigger the logic power control circuit about 400 msec before the data pulses appear. Figure B-1 is a diagram of the modified telemetry format. Figure B-2 is a circuit diagram of the power control circuit.

Figure B-3 is a photograph showing the modified canister. The initial telemetry data indicated that a spin-axis conversion had occurred. The system ran for 140 days. The temperature and voltage data were very close to the predicted theoretical values.

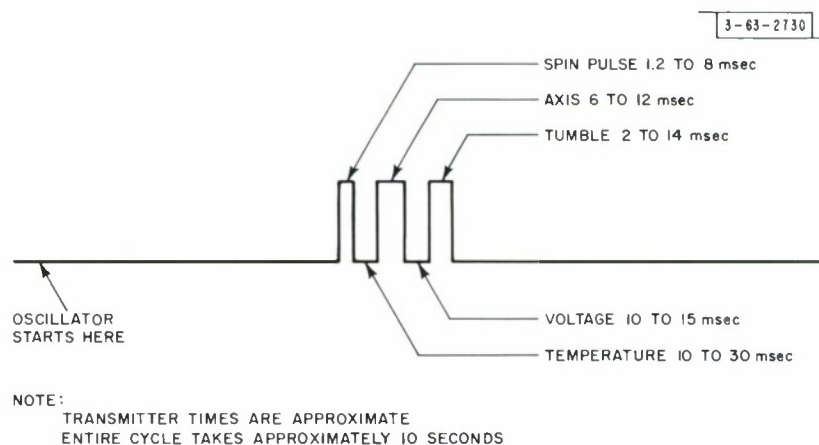
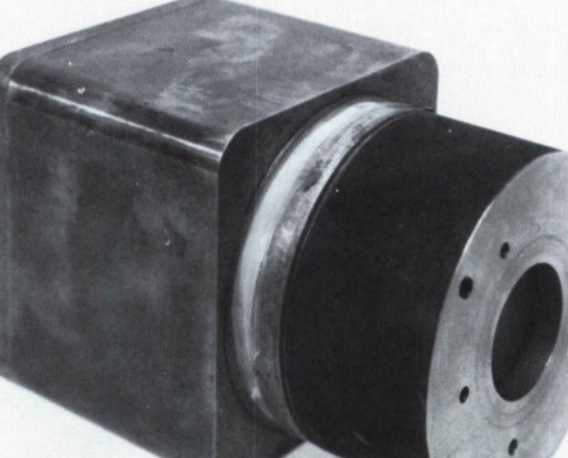
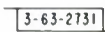


Fig. B-1. Modified square canister telemetry format.



P740-824

Fig. B-3. Modified square canister.

APPENDIX C

LOGIC CIRCUITRY CONSIDERATIONS

I. ONE-SHOT MULTIVIBRATOR POWER

The relative power consumed by 2-, 3-, and 4-transistor one-shot MVs are

$$\text{2-transistor power} = P_2 \approx V_+^2 \left(\frac{1}{R_C} + \frac{1 + 1.5D}{R_N} \right) \quad (C-1)$$

$$\text{3-transistor power} = P_3 \approx V_+^2 \left(\frac{D}{R_C} + \frac{D}{R_P} + \frac{1 + 2.5D}{R_N} \right) \quad (C-2)$$

$$\text{4-transistor power} = P_4 \approx V_+^2 \left(\frac{1}{R_P} + \frac{D}{R_P} + \frac{1 + 2.5D}{R_N} \right) \quad , \quad (C-3)$$

where

R_P = effective series base resistance of PNP

R_N = effective series base resistance of NPN

R_C = effective collector resistance

D = duty cycle ($0 \leq D \leq 1$).

It has been assumed that the timing is performed at the bases of the NPNs and that all circuits are symmetrical with respect to their base and collector resistors. If it is further assumed that $R_N = R_P = 10R_C$, i.e., design $\beta = \beta_d = 10$, and if P_2 , P_3 , and P_4 are normalized by the power of the 4-transistor MV, then

$$\text{relative 2-transistor power} = \frac{11 + 1.5D}{2 + 2.5D} = P_2/P_4 \quad 6.5 \geq P_2/P_4 \geq 3 \quad , \quad (C-4)$$

$$\text{relative 3-transistor power} = \frac{1 + 13.5D}{2 + 2.5D} = P_3/P_4 \quad 3.3 > P_3/P_4 \geq 1/2 \quad , \quad (C-5)$$

$$\text{relative 4-transistor power} = 1 \quad .$$

Note that $P_3/P_4 = 1$ for $D = 9$ percent so that for the duty cycles used in these MVs (≈ 1 percent) the 3-transistor is not only simpler, but also nearly twice as efficient as the 4-transistor MV. The duty cycle for which the $P_3 = P_4$ as a function of the design β_d of the MV is

$$D = \frac{1}{\beta_d + 1} \quad . \quad (C-6)$$

II. DISPENSING RATE TIMING CIRCUIT

Figures C-1 to C-3 show the equivalent recovery circuit and the associated recovery waveform for the sublimation MV. The equation for the normalized recovery time is derived as

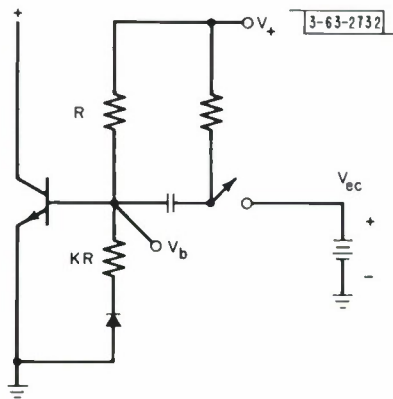
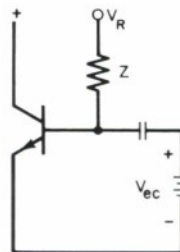


Fig. C-1. Equivalent circuit for sublimation multivibrator immediately prior to triggering.

Fig. C-2. Equivalent circuit for sublimation multivibrator during recovery.



DURING FIRST PART OF RECOVERY:
(during T_A) $V_R = \frac{KV_+ - V_D}{K+1}$

$$Z = \frac{KR}{K+1}$$

DURING SECOND PART OF RECOVERY:
(during T_B) $V_R = V_+$
 $Z = R$

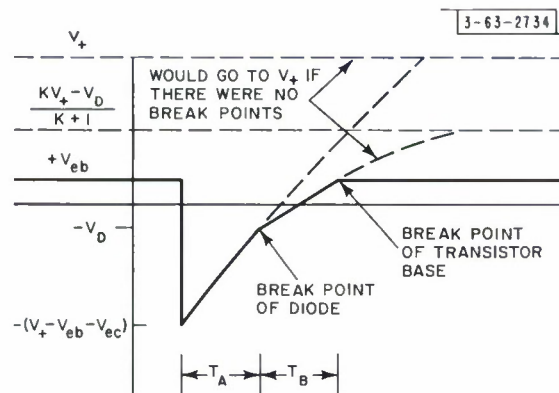


Fig. C-3. Base recovery voltage V_1 for sublimation multivibrator.

$$T_n = \frac{(K + 1) \ln \left(\frac{V_+ + V_D}{V_+ - V_{eb}} \right) + K \ln \left[\frac{(2K + 1) V_+ - (K + 1) (V_{eb} + V_{ec}) - V_D}{K(V_+ + V_D)} \right]}{(K + 1) \ln \left(\frac{2V_+ - V_{eb} - V_{ec}}{V_+ - V_{eb}} \right)} \quad (C-7)$$

where

T_n = normalized recovery time

V_+ = supply voltage

V_D = diode voltage

K = ratio of switched resistor to usual time constant resistor

V_{eb} = emitter-base voltage during conduction

V_{ec} = emitter-to-collector saturation voltage.

The solution of Eq. (C-7) is a function of the supply voltage and power level of operation. The latter controls the values of V_{ec} , V_{eb} , and V_D used in this equation.

For the power levels which this particular circuit operates, the saturation voltages of $V_{ec} = 0.2$, $V_{eb} = 0.5$, and $V_D = 0.5$ are encountered. A graphical solution of Eq. (C-7) with these values and for $V_+ = +6$, yields K values at the $T_a = \frac{3}{4}$ -, $\frac{1}{2}$ -, and $\frac{1}{4}$ -times of 0.4, 0.09, and 0.002. This indicates that for the normal recovery resistance of 200 kohms, the resistors switched in at the different stages of sublimation should be 80 kohms, 24 kohms, and 400 ohms, respectively. The actual values used (determined experimentally) were 100, 33, and 1 kohms, respectively.

APPENDIX D

ANTENNA PHASING NETWORK

Two transmission lines of characteristic impedance Z_o and of lengths ℓ_1 and ℓ_2 are wanted with the requirement that when the inputs to the lines are fed in parallel, the currents through equal, decoupled terminating loads of impedance Z_R are equal in amplitude and in phase quadrature.

Starting with Eq. 4.43*

$$Z_{tr} = \frac{E_S}{I_R} = Z_R \cosh \gamma \ell + Z_o \sinh \gamma \ell \quad , \quad (D-1)$$

where

Z_{tr} = transfer impedance

E_S = sending end voltage

I_R = receiving end current

Z_R = load impedance (receiving end)

Z_o = transmission line characteristic impedance

$\gamma = \alpha + j\beta$ = propagation constant

ℓ = line length

$$I_R = \frac{E_S}{Z_R \cosh \gamma \ell + Z_o \sinh \gamma \ell} \quad .$$

For lines with negligible loss ($\alpha \ell \approx 0$), $\cosh \gamma \ell \approx \cos \beta \ell$, $\sinh \gamma \ell \approx j \sin \beta \ell$, and

$$I_R = \frac{E_S}{Z_R \cos \beta \ell + j Z_o \sin \beta \ell} \quad . \quad (D-2)$$

If the two inputs are fed in parallel $E_{S1} = E_{S2}$. Then,

$$\frac{I_{R1}}{I_{R2}} = \frac{Z_R \cos \beta \ell_2 + j Z_o \sin \beta \ell_2}{Z_R \cos \beta \ell_1 + j Z_o \sin \beta \ell_1} \quad (D-3)$$

$$\begin{aligned} &= \frac{Z \cos \beta \ell_2 + j \sin \beta \ell_2}{Z \cos \beta \ell_1 + j \sin \beta \ell_1} \\ &= \frac{r \cos \beta \ell_2 + j(x \cos \beta \ell_2 + \sin \beta \ell_2)}{r \cos \beta \ell_1 + j(x \cos \beta \ell_1 + \sin \beta \ell_1)} \quad , \end{aligned} \quad (D-4)$$

* W. C. Johnson, Transmission Lines and Networks (McGraw-Hill, New York, 1950).

where

$$Z = \frac{Z_R}{Z_O} = r + jx \quad ,$$

$$I_{R1} = |I_{R1}| \angle \arg I_{R1}$$

and

$$I_{R2} = |I_{R2}| \angle \arg I_{R2} \quad .$$

We want

$$|I_{R1}| = |I_{R2}| \tag{D-5}$$

and

$$\arg I_{R1} - \arg I_{R2} = \pm 90^\circ \quad . \tag{D-6}$$

The ratio I_{R1}/I_{R2} is the ratio of two phasors

$$\frac{r \cos \beta l_2 + j(x \cos \beta l_2 + \sin \beta l_2)}{r \cos \beta l_1 + j(x \cos \beta l_1 + \sin \beta l_1)} \quad .$$

Equation (D-5) says that the two phasors should be of equal amplitude; thus

$$(r \cos \beta l_2)^2 + (x \cos \beta l_2 + \sin \beta l_2)^2 = (r \cos \beta l_1)^2 + (x \cos \beta l_1 + \sin \beta l_1)^2 \quad . \tag{D-7}$$

Equation (D-6) says that the two phasors, when drawn geometrically in the complex plane, should be at right angles; thus

$$\frac{x \cos \beta l_2 + \sin \beta l_2}{r \cos \beta l_2} = \frac{-r \cos \beta l_1}{x \cos \beta l_1 + \sin \beta l_1} \quad . \tag{D-8}$$